Supporting Information

for

Facile synthesis of compact CdS−CuS heterostructures for optimal CO_2−to−syngas photoconversion

Jian–Ying Xu[a], Xiang–Ji Liu[a], Han–Nan Huang[a], Yu–Hang Xu[a], Zhou Zhong[a,*], Ya–Feng Li[b], Raymond Jianxiong Zeng[a], Jian Lü[a,b,c*] and Rong Cao[c]

[a]Fujian Provincial Key Laboratory of Soil Environmental Health and Regulation, College of Resources and Environment, Fujian Agriculture and Forestry University, No. 15 Shang Xia Dian Road, Fuzhou 350002, P.R. China; [b]State Key Laboratory of Photocatalysis on Energy and Environment, Fuzhou University, No. 2 Xue Yuan Road, Fuzhou 350116, P.R. China; [c]State Key Laboratory of Structural Chemistry, Fujian Institute of Research on the Structure of Matter, Chinese Academy of Sciences, Fuzhou 350002, P.R. China.

*E–mail: zhongzhou91@126.com (Z.Z.); jian_lu_fafu@163.com (J.L.)

Number of tables: 6

Number of figures: 11

Table of Contents

1. Supplementary Materials and Methods

1.1 Reagents

All of the chemicals and solvents in this work were used as received without further purification. Thiourea was bought from Shanghai Macklin Biochemical Technology Co., Ltd. Triethanolamine (TEOA, 99.8%), acetonitrile (MeCN, 99.9%), $Cu(NO_3)_2{\cdot}3H_2O$ and ethylene glycol (EG) were purchased from Sinopharm Chemical Reagent Co., Ltd. (China). Ethylenediamine (> 99.5%), $Cd(NO_3)_2{\cdot}4H_2O$ and Na_2SO_4 were purchased from Aladdin Ltd. (Shanghai, China). $Na_2S.9H_2O$ (99.5%) was bought from Shanghai Titan Scientific Co., Ltd. Reaction solutions and stock solutions were prepared by using deionized water supplied with a UPT–I–5T ultrapure water system.

1.2 Characterizations

The crystal structure was characterized by X–ray powder diffraction (PXRD) by using a PANalytical X'PertPRO diffractometer (Cu radiation, $\lambda = 0.154$ nm) operated at 40 kV and 40 mA (PANalytical, Holland) in 2θ range of 10–80°. Scanning electron microscopy (SEM) images were photographed by using a SU8020 with a working voltage of 10 kV. Transmission electron microscopy (TEM) and high–resolution TEM (HR–TEM) images were recorded by using a Tecnai G2 F30 S–TWIN working at 200 kV. The inter–planer distances and the inverse Fast Fourier Transform (FFT) were calculated using the Digital Micrograph software. X–ray photoelectron spectroscopy (XPS) measurements were performed on a Thermo Fisher ESCALAB 250Xi spectrometer with Al Kα X–ray source (15 kV, 10 mA). In order to compensate effects related to charge shifts C 1s peak at 284.8 eV was used as internal standard. Diffuse reflectance spectra (DRS) were recorded on a Shimadzu UV–vis spectrophotometer (UV–2600) with $BaSO_4$ as the background. The photoluminescence (PL) and time-resolved PL spectra were collected on a FLS 1000 fluorescence spectrometer at room temperature, moreover the excitation wavelength was 350 nm. Cd and Cu were determined using a Jobin Yvon Ultima2 inductively coupled plasma atomic emission spectrometer (ICP–AES). The specific surface area was determined by the Brunauer–Emmett–Teller (BET) method with N_2 adsorption at 77 K (TriStar II 3020).

2. Supplementary Tables

Table S1. ICP–AES results of the CdS–CuS–x (x = 1/2/3/4/5).

Composite photocatalyst	Cd (mol%)	Cu (mol%)	Cd : Cu (molar ratio)
CdS–CuS–1	46.0	10.5	1 : 0.23
CdS–CuS–2	42.8	13.7	1 : 0.32
CdS–CuS–3	37.6	18.7	1 : 0.5
CdS–CuS–4	25.8	26.6	1 : 1.0
CdS–CuS–5	6.45	55.0	1 : 8.5

Table S2. ICP–AES results of the CdS/CuS–x (x = 1/2/3/4/5).

Composite photocatalyst	Cd (mol%)	Cu (mol%)	Cd : Cu (molar ratio)
CdS/CuS–1	63.6	8.6	1:0.14
CdS/CuS–2	59.9	14.1	1:0.24
CdS/CuS–3	55.9	20.3	1:0.36
CdS/CuS–4	50.4	27.8	1:0.55
CdS/CuS–5	42.1	41.2	1:0.97

Table S3. BET surface area results of the CdS, CdS–CuS–2, CdS/CuS–2 and CuS.

Photocatalyst	BET surface area ($m^2\ g^{-1}$)
CdS	25.2
CuS	26.9
CdS–CuS–2	26.4
CdS/CuS–2	24.8

Table S4. Rations of H_2/CO of the CdS–CuS photocatalytic reduction of CO_2 to syngas.

Composite photocatalyst	H_2 production rate ($\mu mol \cdot h^{-1} \cdot g^{-1}$)	CO production rate ($\mu mol \cdot h^{-1} \cdot g^{-1}$)	H_2:CO
CdS–CuS–1	1499.8	45.3	33:1
CdS–CuS–2	2416.5	203.4	12:1
CdS–CuS–3	1251.6	98.9	13:1
CdS–CuS–4	487.0	23.6	21:1
CdS–CuS–5	16.0	18.5	1:1

Table S5. Rations of H_2/CO of the CdS/CuS photocatalytic reduction of CO_2 to syngas.

Composite photocatalyst	H_2 production rate ($\mu mol \cdot h^{-1} \cdot g^{-1}$)	CO production rate ($\mu mol \cdot h^{-1} \cdot g^{-1}$)	H_2:CO
CdS/CuS–1	1213.0	13.5	90:1
CdS/CuS–2	1329.6	34.4	39:1
CdS/CuS–3	1319.2	33.9	39:1
CdS/CuS–4	1143.4	27.3	42:1
CdS/CuS–5	561.7	20.8	27:1

Table S6. Comparison of various CdS–based catalysts for the photocatalytic CO_2 reduction.

Photocatalyst	Sacrificial agent	CO production rate	CH_4 production rate	Reference
ZnS/CdS/rGO	TEOA	9.69	/	S1
CdS/Ni(bpy)$_3$Cl$_2$	TEOA	46.9	/	S2
CdS/TiO$_2$	/	3.62	/	S3
CdS/CdV$_2$O$_6$	Na_2S/Na_2O_3	/	2.98	S4
CdS/Ni$_9$S$_8$/Al$_2$O$_3$	TEOA	121	/	S5
CdS/NH$_2$–UiO–66/chitosan	TEOA	96.98	/	S6
CdS/FeTCPP	TEOA	7.16	/	S7
Ni/CdS QDs	TEOA	9.5	1.1	S8
NG/CdS	/	2.6	0.3	S9
FeOOH/CdS	/	12.55	5.88	S10
CdS–CuS	TEOA	203.4 ± 15.7	2.8 ± 0.3	this work

3. Supplementary figures

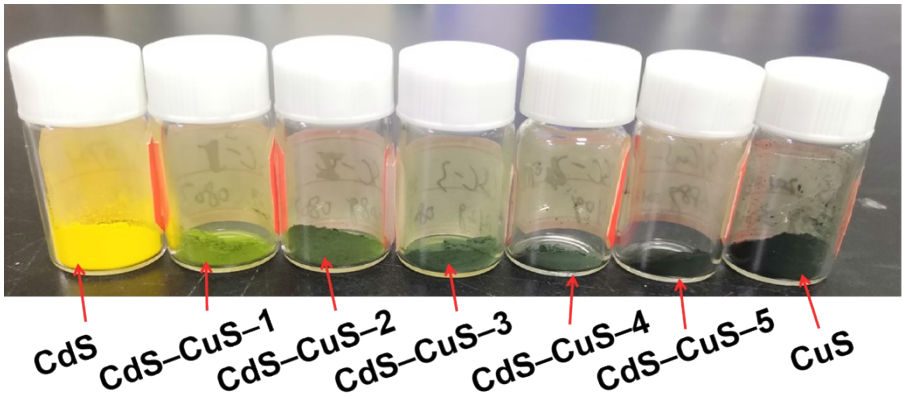

Fig. S1. Photographs of as–prepared materials.

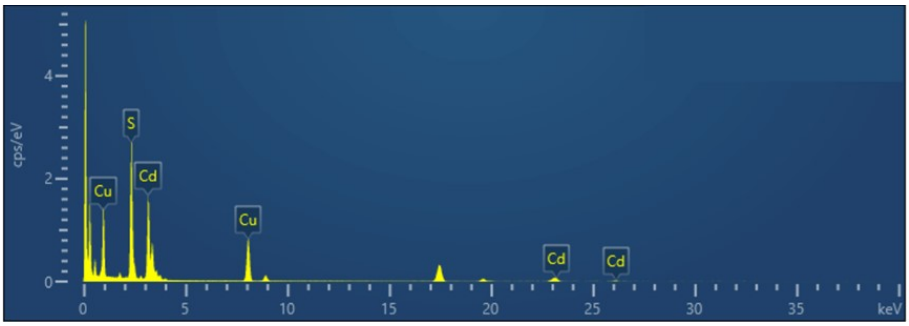

Fig. S2. EDX spectrum of CdS–CuS–2.

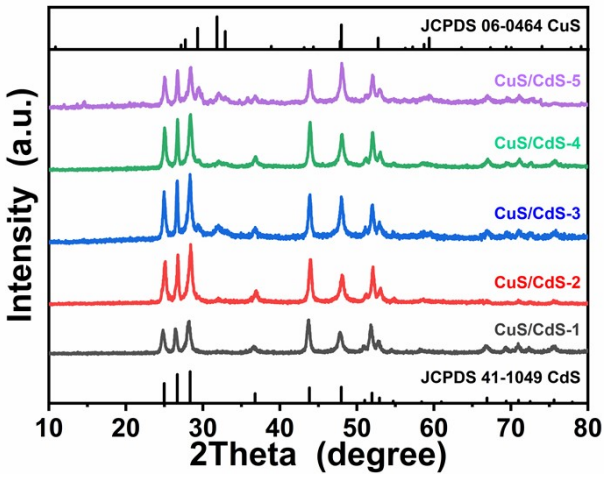

Fig. S3. PXRD of the as–prepared samples of CdS/CuS–x (x = 1/2/3/4/5).

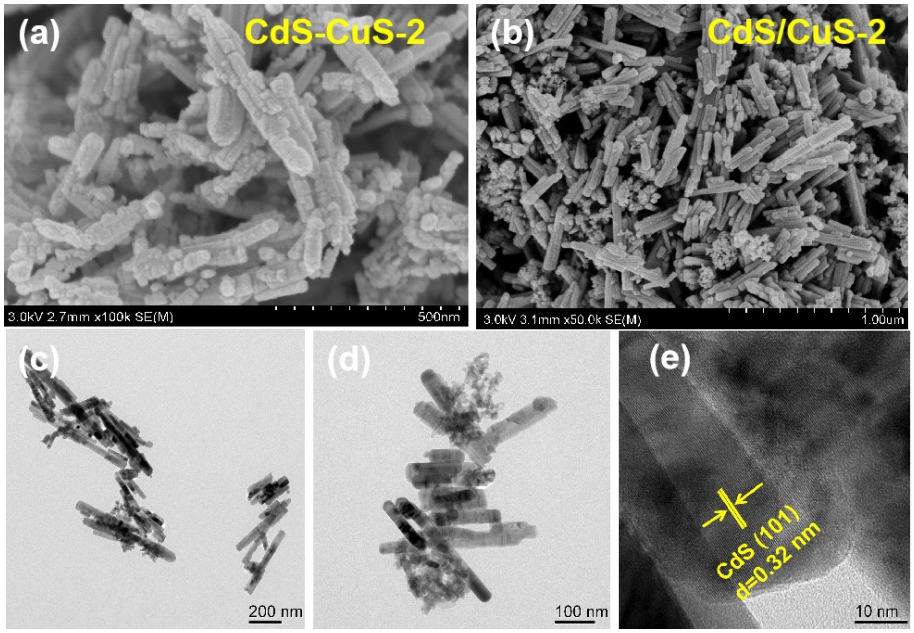

Fig. S4. (a) SEM images of CdS–CuS–2; (b) SEM images of CdS/CuS–2 (c, d) TEM images of CdS/CuS–2; (e) HRTEM of CdS/CuS–2.

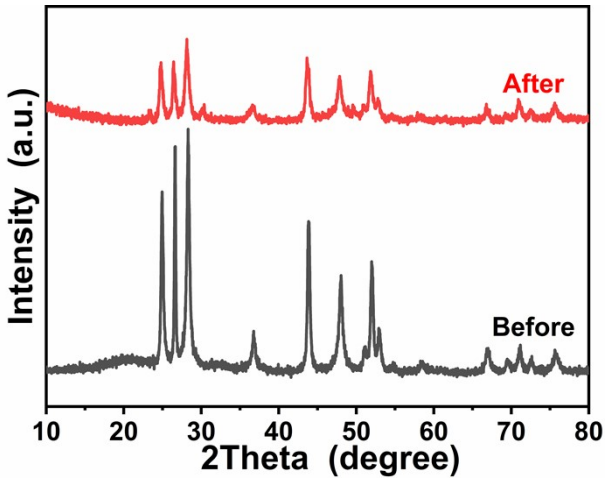

Fig. S5. PXRD of the as–prepared and recycled samples of CdS–CuS–2.

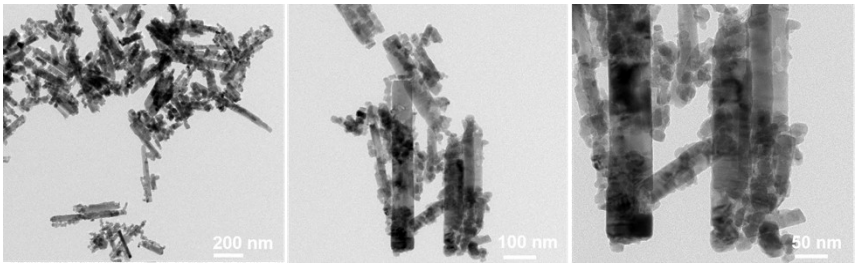

Fig. S6. TEM images of CdS−CuS−2 after photocatalytic reactions.

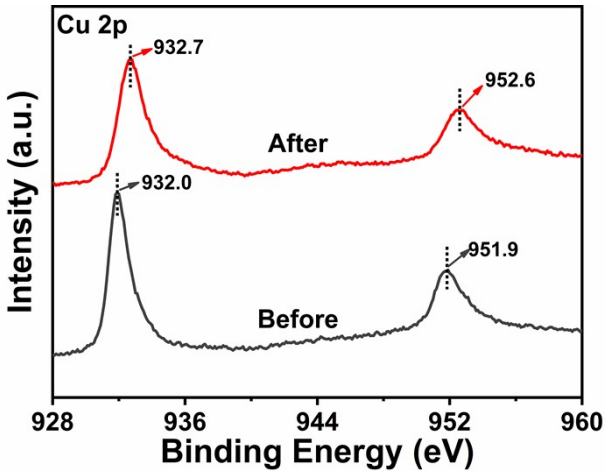

Fig. S7. High–resolution XPS spectra of Cu 2p spectra of the as–prepared and recycled samples of CdS–CuS–2.

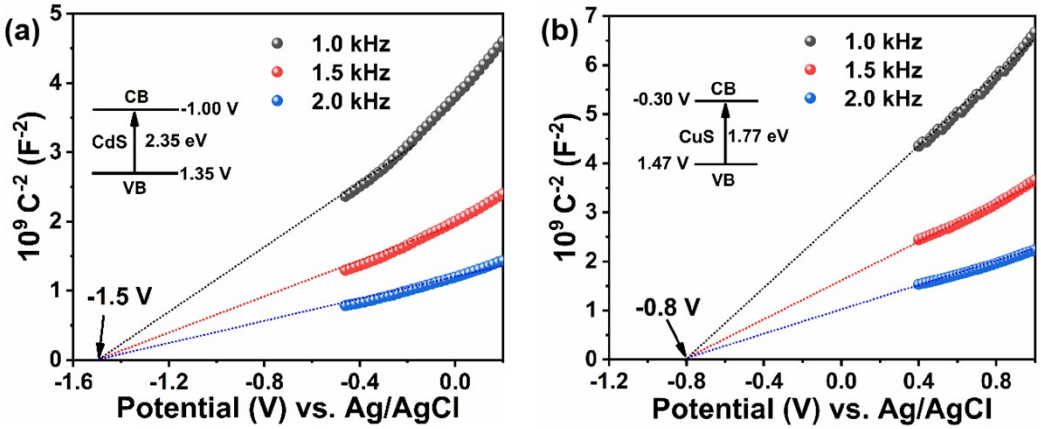

Fig. S8. Mott–Schottky plots of CdS (a) and CuS (b).

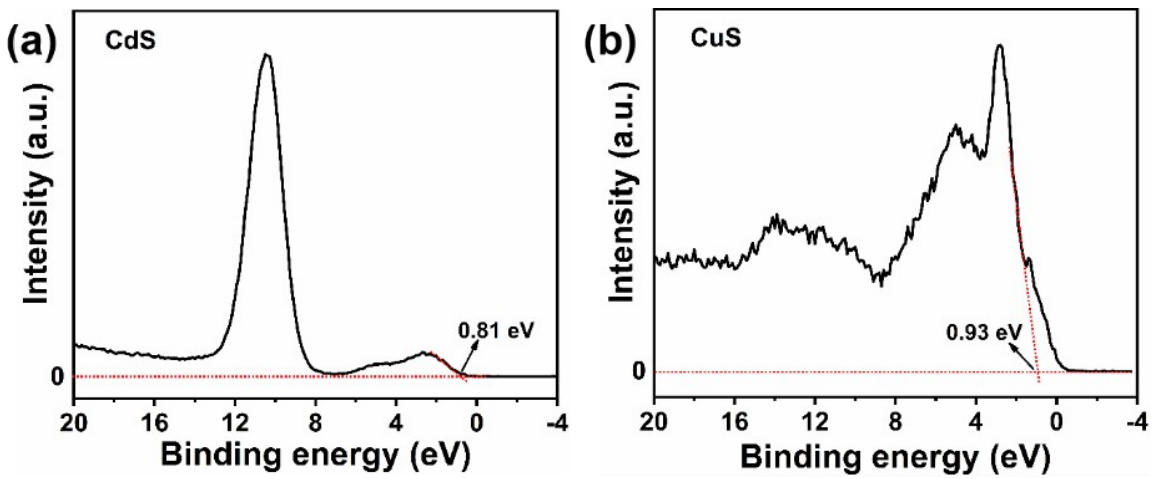

Fig. S9. VB–XPS curves of CdS (a) and CuS (b).

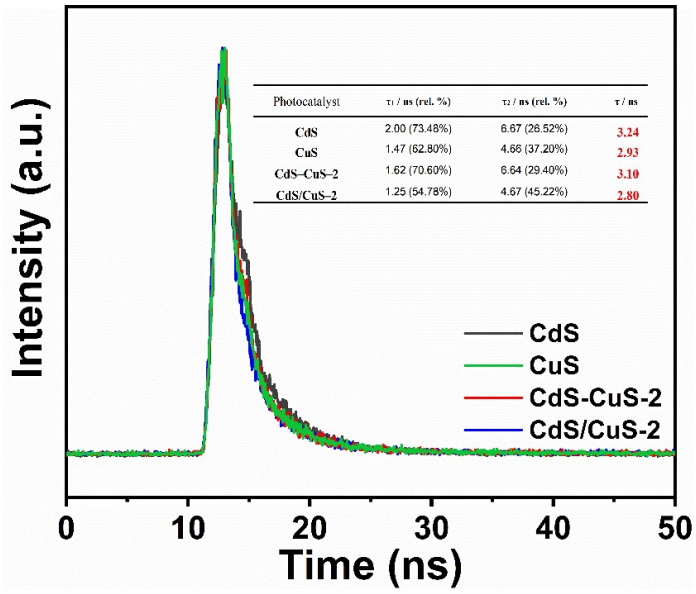

Fig. S10. Time–resolved PL spectra of CdS, CuS, CdS–CuS–2 and CdS/CuS–2.

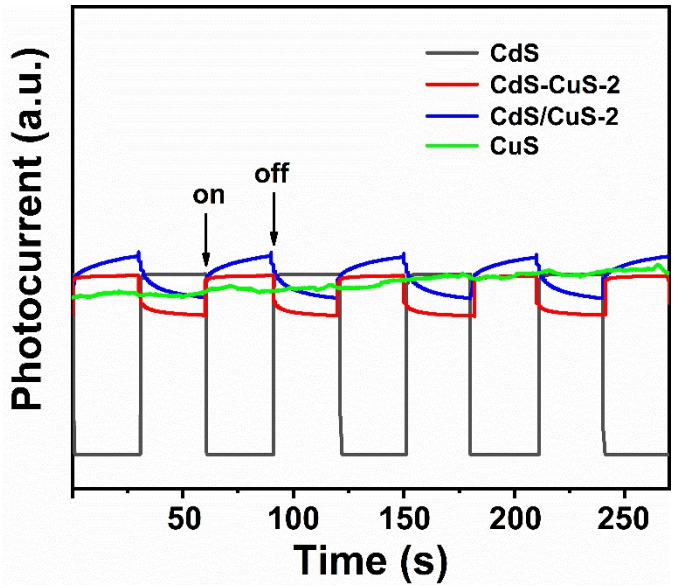

Fig. S11. Transient photocurrent response plots of CdS, CuS, CdS–CuS–2 and CdS/CuS–2.

4. Supplementary reference

S1. M. Xu, H. Jiang, X. Li, M. Gao, Q. Liu, H. Wang, P. Huo and S. Chen, Design of a ZnS/CdS/rGO composite nanosheet photocatalyst with multi–interface electron transfer for high conversion of CO_2, *Sustainable Energy Fuels*, 2021, **5**, 4606–4617.

S2. J. Lin, B. Qin and Z. Fang, Nickel Bipyridine ($Ni(bpy)_3Cl_2$) Complex used as molecular catalyst for photocatalytic CO_2 reduction, *Catal. Lett.*, 2019, **149**, 25–33.

S3. X. Pan and Y.–J. Xu, Graphene–templated bottom–up fabrication of ultralarge binary CdS–TiO_2 nanosheets for photocatalytic selective reduction, *J. Phys. Chem. C*, 2015, **119**, 7184–7194.

S4. S. Ijaz, M. F. Ehsan, M. N. Ashiq, N. Karamt, M. Najam–ul–Haq and T. He, Flower–like CdS/CdV_2O_6 composite for visible–light photoconversion of CO_2 into CH_4, *Mater. Des.*, 2016, **107**, 178–186.

S5. S. Li, Q. Wang, X. Yan, H.–Q. Zhuang, C. Yuan, J. Feng, M. Wang, R. Li, W. Li and Y.–X. Pan, Al_2O_3 support triggering highly efficient photoreduction of CO_2 with H_2O on noble–metal–free $CdS/Ni_9S_8/Al_2O_3$, *Appl. Catal., B*, 2019, **240**, 174–181.

S6. H. Zhao, X. Yang, R. Xu, J. Li, S. Gao and R. Cao, CdS/NH_2–UiO–66 hybrid membrane reactors for the efficient photocatalytic conversion of CO_2, *J. Mater. Chem. A*, 2018, **6**, 20152–20160.

S7. P. Li, C. Hou, X. Zhang, Y. Chen and T. He, Ethylenediamine–functionalized CdS/tetra(4–carboxyphenyl)porphyrin iron(III) chloride hybrid system for enhanced CO_2 photoreduction, *Appl. Surf. Sci.*, 2018, **459**, 292–299.

S8. J. Wang, T. Xia, L. Wang, X. Zheng, Z. Qi, C. Gao, J. Zhu, Z. Li, H. Xu and Y. Xiong, Enabling Visible–Light–Driven Selective CO_2 reduction by doping quantum dots: trapping electrons and suppressing H_2 evolution, *Angew. Chem., Int. Ed.*, 2018, **57**, 16447–16451.

S9. C. Bie, B. Zhu, F. Xu, L. Zhang and J. Yu, In situ grown monolayer N–doped graphene on CdS hollow spheres with seamless contact for photocatalytic CO_2 reduction, *Adv. Mater.*, 2019, **31**, 1902868.

S10. L. Li, C. Guo, J. Ning, Y. Zhong, D. Chen and Y. Hu, Oxygen–vacancy–assisted construction of FeOOH/CdS heterostructure as an efficient bifunctional photocatalyst for CO_2 conversion and water oxidation, *Appl. Catal., B*, 2021, **293**, 120203.